Seismic performance of base-isolated buildings under multi-directional earthquake excitations

Noroozinejad Farsangi, Ehsan; Tasnimi, Abbas Ali; Yang, T. Y.; Takewaki, Izuru; Mohammadhasani, Mohammad

Seismic Performance of Base-Isolated Buildings under Multi-Directional Earthquake Excitations

E. Noroozinejad Farsangi[1], A.A. Tasnimi[2], T.Y. Yang*[3,4], Izuru Takewaki[5]
[1]*Department of Earthquake Engineering, KGUT, Kerman, Iran*
[2]*Department of Civil and Environmental Engineering, Tarbiat Modares University, Tehran, Iran*
[3]*International Joint Research Laboratory of Earthquake Engineering, Tongji University, Shanghai, China*
[4]*Department of Civil Engineering, University of British Columbia, Vancouver, Canada*
[5]*Department of Architecture and Architectural Engineering, Graduate School of Engineering, Kyoto University, Kyoto, Japan*

Abstract. Traditional base isolation systems focus on isolating the seismic response of a structure in the horizontal direction. However, in regions where the vertical earthquake excitation is significant (such as near-fault region), a traditional base-isolated building exhibits a significant vertical vibration. To eliminate this shortcoming, a rocking-isolated system named Telescopic Column (TC) is proposed in this paper. Detailed rocking and isolation mechanism of the TC system is presented. The seismic performance of the TC is compared with the traditional elastomeric bearing (EB) and friction pendulum (FP) base-isolated systems. A 4-storey reinforced concrete moment-resisting frame (RC-MRF) is selected as the reference superstructure. The seismic response of the reference superstructure in terms of column axial forces, base shears, floor accelerations, interstory drift ratios (IDR) and collapse margin ratios (CMRs) are evaluated using OpenSees. The results of the nonlinear dynamic analysis subjected to multi-directional earthquake excitations show that the superstructure equipped with the newly proposed TC exhibits a superior response with higher margin of safety against collapse when compared with the same superstructure with the traditional base-isolation (BI) system.

Keywords: Base Isolation, Structural Fuse, Repairable Structure, Fragility Curve, CMR, OpenSees

1. Introduction

Seismic isolations have been used widely in the region of high-seismic activities. They have been proven to provide adequate protection for both structural and non-structural components [1-4]. However, some studies [5-8] have demonstrated that traditional base-isolation devices have large vertical stiffness, which could cause high vertical acceleration and impose significant damages to structural and non-structural elements. This is particularly important for structures located in near-fault region, where vertical excitation is significant. To eliminate the shortcoming of the vertical excitation for base isolated buildings, an innovative structural system named Telescopic Column (TC) is proposed in this paper. Figure 1 shows the concept of the TC structure. In the proposed system, a repairable massive central column (RMCC) is added to allow the superstructure to rock around this point. As the structure rocks, the TCs are designed to deform and engage the Multiple Yielding Plate Energy Dissipating (MYPED) device [9]. Each of the MYPED is a combination of multiple ADAS [10,11] energy dissipating devices, which is designed to dissipate the sudden surge of earthquake energy, while the rest of the structure is protected from the earthquake damage. The ADAS devices are designed to be easily inspected, repaired or replaced after a strong earthquake, which makes the TC structure an effective next-generation earthquake resilient structure. To ensure that the entire superstructure can isolate and rock at its base, a rigid high strength steel (St 52 DIN 17100 steel grade) chassis is added at the base of the superstructure. The rigid high strength chassis is designed to connect to the RMCC to allow the superstructure to rotate and slide around the connection between the RMCC and rigid chassis.

*Corresponding author, Professor, E-mail: yang@ilee-tj.com, yang@civil.ubc.ca

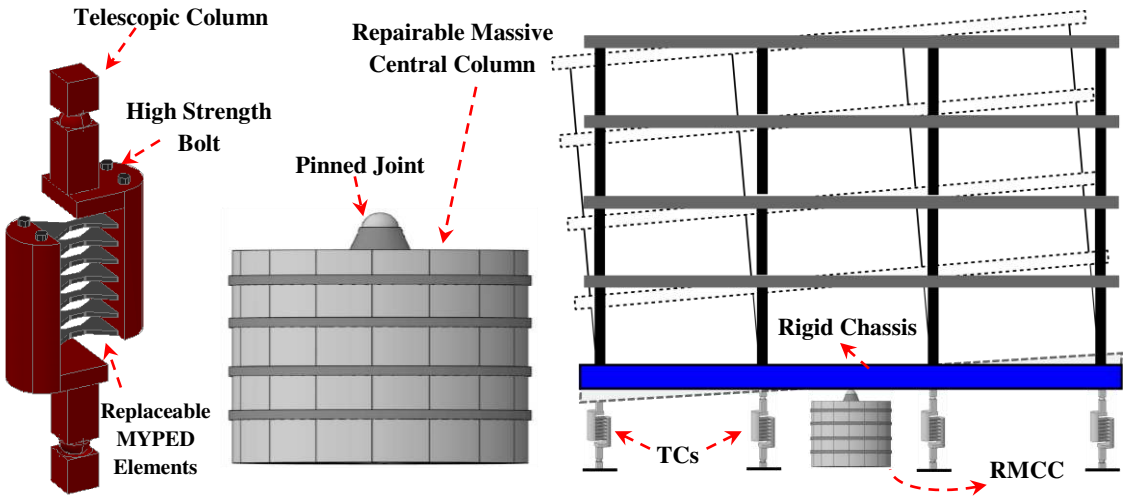

Fig. 1 Schematic representation of the proposed system

To examine the dynamic response of the TC system, an analytical model for the TC structure under multidirectional earthquake excitations is derived. The analytical model is used to size the MYPED. To demonstrate the effectiveness of the TC structural system under combined horizontal and vertical excitations, a 4-storey reinforced concrete moment-resisting frame (RC-MRF) is selected as the reference superstructure. Detailed finite element model of the prototype building is developed using OpenSees [12] and the seismic response is compared with the same superstructure with traditional friction pendulum (FP) and elastomeric bearing (EB) isolation systems. The results of the nonlinear dynamic analysis subjected to multi-directional earthquake excitations show that the superstructure equipped with the newly proposed TC exhibits a superior response with higher margin of safety against collapse when compared with the same superstructure with the traditional base-isolation (BI) system.

2. Dynamic equilibrium equations of the TC system

Figure 2 shows the equations of motion derived for an *n*-story, 1-bay TC structure. For simplicity, the floor diaphragms are assumed to be rigid and the axial deformations in columns are neglected. Combined horizontal and vertical ground excitations are applied to the structure simultaneously. Eqns. 1 and 2 depict the relative inter-story drifts of the 1st and nth story, respectively. Note that these quantities do not include the rigid body rotation caused by the foundation rocking.

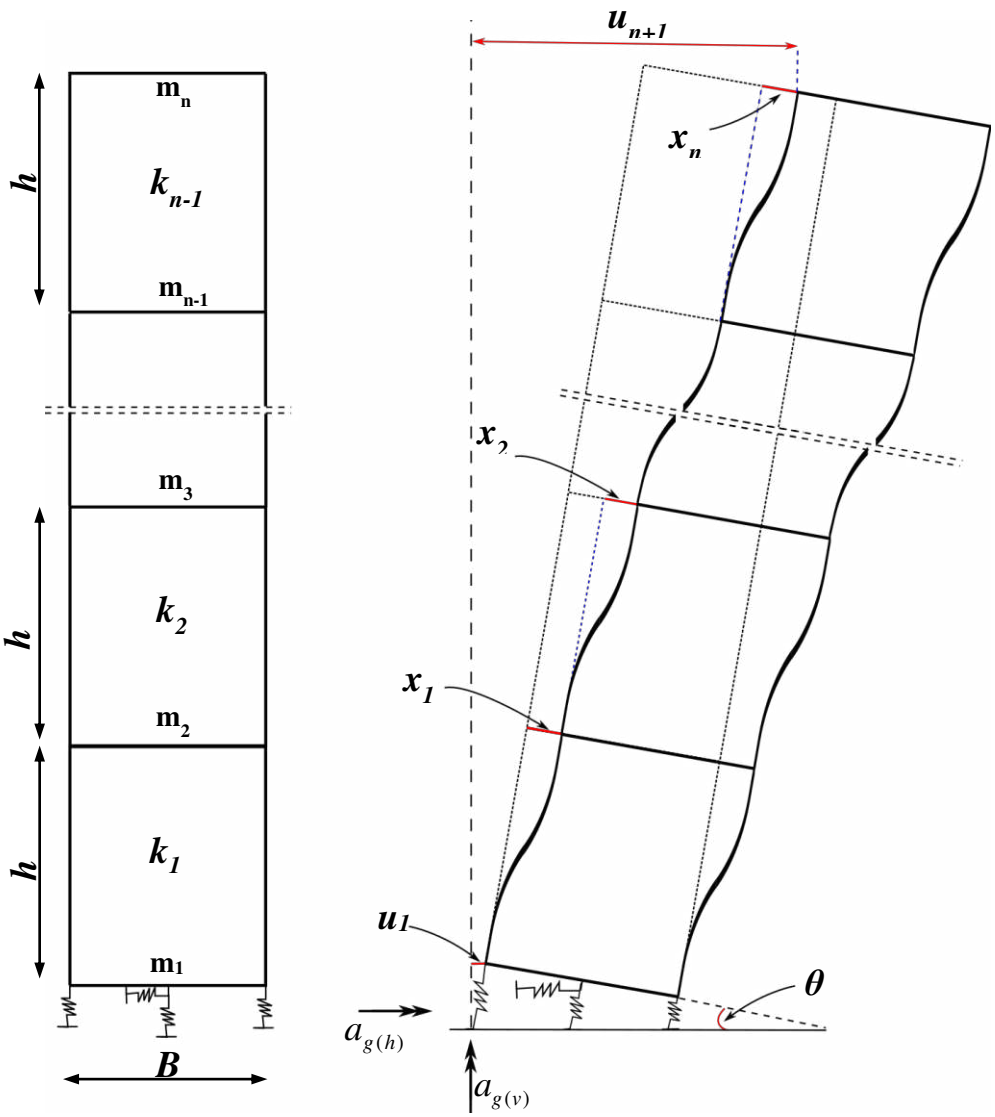

Fig. 2 Illustration of the dynamic response of a multi-storey building equipped with proposed system

$$x_1 = u_2 - u_1 - h\theta \tag{1}$$

$$x_n = u_{n+1} - u_n - h\theta \tag{2}$$

Based on above Eqns., the moments at 1st and n^{th} floors can be calculated as:

$$M_1 = \frac{k_1(u_2 - u_1 - h\theta) \times h}{4} \tag{3}$$

$$M_n = \frac{k_n(u_{n+1} - u_n - h\theta) \times h}{4} \tag{4}$$

The equilibrium conditions for 1st and n^{th} floor diaphragms can be written as follows:

$$\begin{cases} \sum Fx_1 = 0 \rightarrow f_{1(h)}(t) - k_{h.CC} \times u_1 - m_1 \times \left(u_1^{"} + a_{g(h)}\right) + k_1 \times \left(u_2 - u_1 - h\theta\right) = 0 \\ \sum Fy_1 = 0 \rightarrow f_{1(v)}(t) - k_{v.CC} \times \left(y_{TC} - y_g\right) - m_1 \times \left(y_{TC}^{"} + a_{g(v)}\right) - k_{TC} \times \left(y_{TC} - y_g\right) = 0 \\ \sum M_1 = 0 \rightarrow M_1(t) + k_1 \times (u_2 - u_1 - h\theta)\frac{h}{2} - m_{\theta 1} \times \theta^{"} - \frac{\theta L^2}{4} \times k_{TC} + P_1 \times B = 0 \end{cases} \quad (5)$$

$$\begin{cases} \sum Fx_n = 0 \rightarrow f_{n(h)}(t) - k_{h.CC} \times u_1 - m_n \times \left(u_n^{"} + a_{g(h)}\right) + k_{n-1} \times \left(u_n - u_{n-1} - h\theta\right) = 0 \\ \sum Fy_n = 0 \rightarrow f_{n(v)}(t) - m_n \times \left(y_{TC}^{"} + a_{g(v)}\right) = 0 \\ \sum M_n = 0 \rightarrow M_n(t) + k_{n-1} \times (u_n - u_{n-1} - h\theta)\frac{h}{2} - m_{\theta n} \times \theta^{"} - P_{n-1} \times B = 0 \end{cases} \quad (6)$$

Based on the above formulation, the equation of motion for the proposed system in the matrix format can be written as Eqn. 7. It should be noted that such formula can be used in the preliminary design of the proposed system to find a suitable range of stiffness for the TCs and RMCC. In the developed equation, the subscripts "*CC*" and "*TC*" are related to the central and telescopic columns, respectively.

$$\begin{pmatrix} m_1 & 0 & \cdots & 0 & 0 & 0 \\ 0 & m_2 & \cdots & 0 & 0 & 0 \\ \vdots & \vdots & \ddots & 0 & 0 & 0 \\ 0 & 0 & 0 & m_n & 0 & 0 \\ 0 & 0 & 0 & 0 & \sum m_{\theta i} & 0 \\ 0 & 0 & 0 & 0 & 0 & \sum m_i \end{pmatrix} \begin{pmatrix} u_1^{"} \\ u_2^{"} \\ \vdots \\ u_n^{"} \\ \theta^{"} \\ y_{TC}^{"} \end{pmatrix} + \left(C\right)_{Raleigh} \begin{pmatrix} u_1^{'} \\ u_2^{'} \\ \vdots \\ u_n^{'} \\ \theta^{'} \\ y_{TC}^{'} - y_g^{'} \end{pmatrix} +$$

$$\begin{pmatrix} k_1 + k_{h.CC} & -k_1 & 0 & \cdots & k_1 h & 0 \\ -k_1 & k_1 + k_2 & -k_2 & \cdots & (k_2 - k_1)h & 0 \\ 0 & -k_2 & \ddots & \ddots & \vdots & \vdots \\ \vdots & \vdots & \ddots & k_{n-1} & -k_{n-1}h & \vdots \\ k_1 h & (k_2 - k_1)h & \cdots & -k_{n-1}h & \sum k_i h^2 + \frac{k_{TC}B^2}{4} & 0 \\ 0 & 0 & \cdots & \cdots & 0 & k_{v.CC} + k_{TC} \end{pmatrix} \begin{pmatrix} u_1 \\ u_2 \\ \vdots \\ u_n \\ \theta \\ y_{TC} - y_g \end{pmatrix}$$

$$= -\left(Mass_{Matrix}\right) \begin{pmatrix} 1 & 0 \\ 1 & 0 \\ 1 & 0 \\ 1 & 0 \\ 0 & 0 \\ 0 & 1 \end{pmatrix} \begin{pmatrix} a_{g(h)} \\ a_{g(v)} \end{pmatrix} \quad (7)$$

3. Description of the Prototype Building:

Figure 3 shows a 4-story RC moment frame office building located in Los Angeles, California which was selected as the prototype superstructure for this study. The building was designed according to ACI-318-89 [13]. The first-mode period of the structure is 0.89 sec. Details of the building design are presented in Table 1.

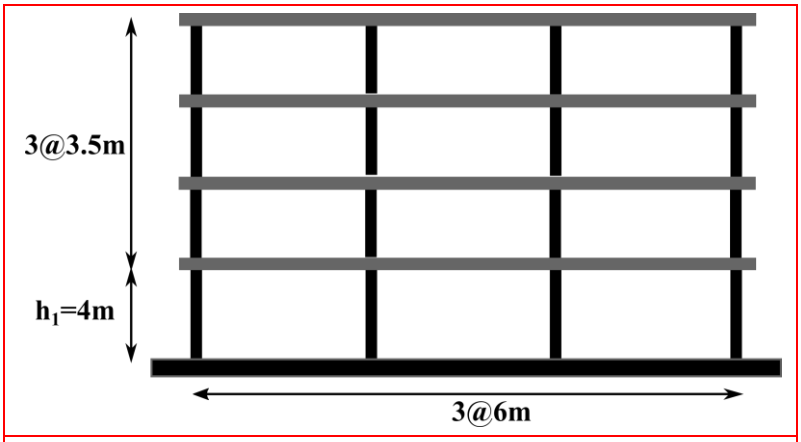

Fig. 3 Schematic presentation of the prototype superstructure

Table 1: Frame element size and reinforcement details

Member	Details	1st Storey	2nd Storey	3rd Storey	4th Storey
Beam	Dimension (b×h), cm×cm	45×60	45×60	45×50	45×50
	Positive longitudinal reinforcement ratio in beams, ρ	0.0054	0.0050	0.0069	0.0072
	Negative longitudinal reinforcement ratio in beams, ρ '	0.0110	0.0100	0.0132	0.0116
	Shear/Transverse reinforcement ratio in beams, ρ_{sh}	0.0025	0.0023	0.0034	0.0032
	Shear/Transverse reinforcement spacing in beams, S(cm)	12.5	12.5	12.5	12.5
Column	Dimension (b×h), cm×cm	65×65	65×65	60×60	60×60
	Total longitudinal reinforcement ratio in columns, ρ_{tot}	0.0160	0.0160	0.0140	0.0110
	Shear/Transverse reinforcement ratio in columns, ρ_{sh}	0.0065	0.0065	0.0065	0.0065
	Shear/Transverse reinforcement spacing in columns, S(cm)	10.0	10.0	10.0	10.0

The seismic response of the superstructure was compared with three isolation schemes, namely: (1) structure with friction pendulums, (2) structure with elastomeric bearings and (3) structure with TC system. Figure 4 shows the three different configurations.

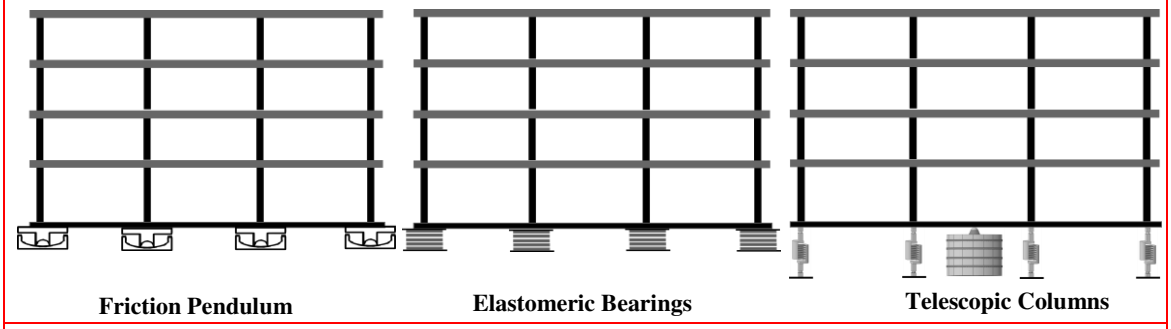

Fig. 4 Reference frame with various base-isolation systems

4. Description of the Analytical Models:

Figure 5 shows the analytical model developed in OpenSees [12]. In this study, the beams/columns were simulated using elastic elements, while the nonlinearity were lumped in the joints region. To model the degradation in these regions, the Hysteresis element within OpenSees developed by [14] was utilized (Figure 6). Nonlinear spring elements were added to the model to simulate the flexural-shear-axial interaction response of moment frame elements. Limit State Material (LSM) was used to model the drift shear interaction [15].

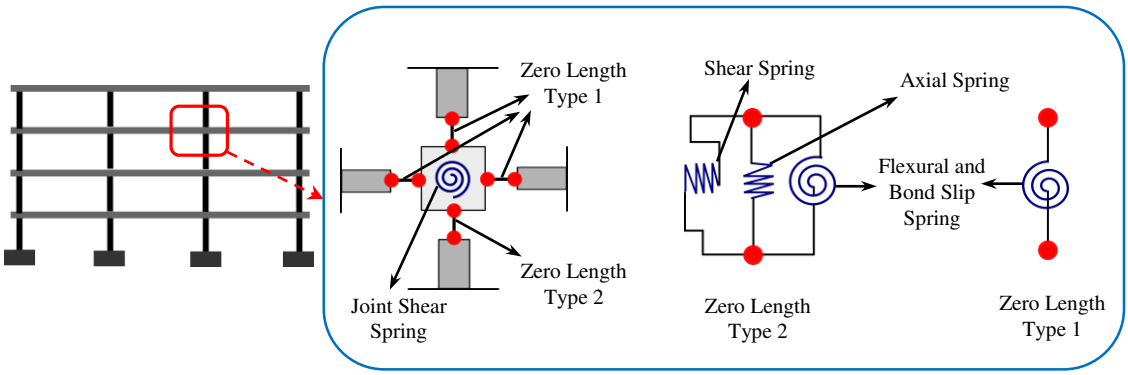

Fig. 5 FE model of superstructure developed in OpenSees

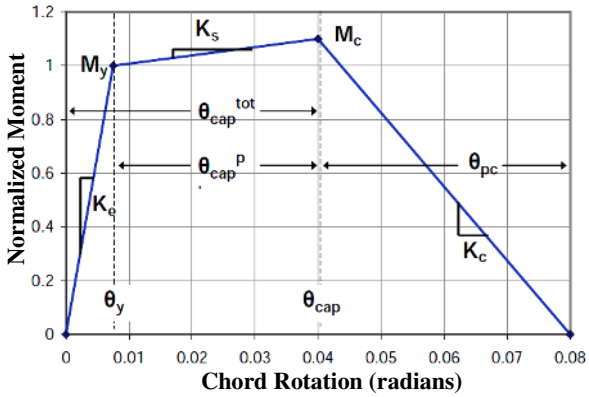

Fig. 6 Monotonic behavior of joint model used in this study [14]

The elastomeric bearing was modeled using the springs and dashpots. This element uses a coupled plasticity model to represent the lateral force-deformation behavior of the bearing that is characterized using the bilinear force-deformation relationship shown in Figure 7. The bi-linear

characterization shown in Figure 7 is defined by the following parameters: Q_d the zero-displacement force-intercept; K_d the second-slope stiffness and K_u the elastic stiffness.

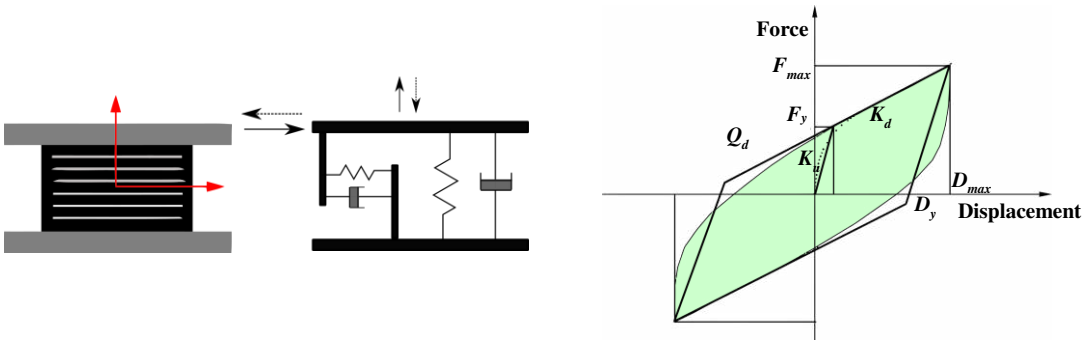

Fig. 7 Elastomeric bearing, idealized physical model and bilinear idealization of isolator unit behavior developed in OpenSees

The friction pendulum (FP) system was modeled using a Flat Slider Bearing model in OpenSees. Figure 8 shows the force-deformation response of the friction pendulum. The force-deformation response of the friction pendulum can be characterized by the characteristic strength Q_d, the coefficient of friction and the instantaneous axial load, the post-yield stiffness K_d, the ratio of the instantaneous axial load and the effective radius of curvature. The axial load on the bearing changes during an earthquake due to the ground motion in the vertical direction and the frame action in the superstructure. Consequently, Q_d and K_d change continuously during an earthquake. The characteristic strength also changes as the coefficient of sliding friction updates with the velocity of sliding, axial pressure on the bearing and the temperature at the sliding surface. The source code for the Flat Slider Bearing element was modified so that the new element would update the coefficient of friction at every step of analysis.

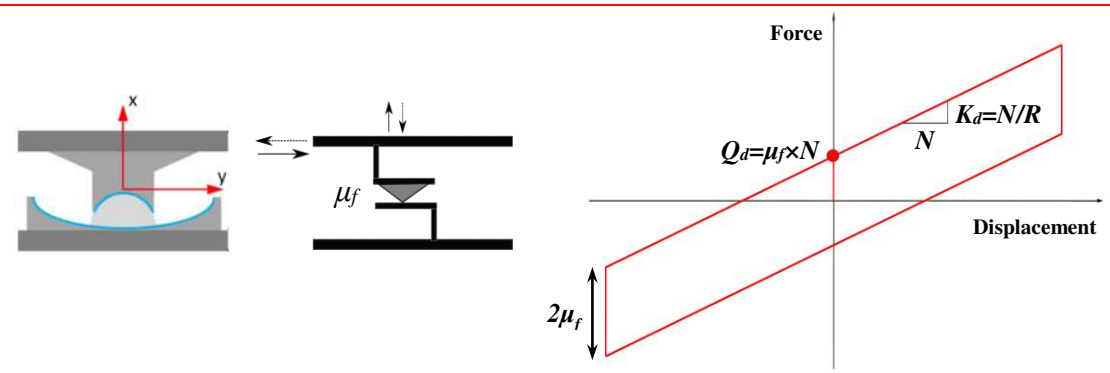

Fig. 8 Friction Pendulum bearing, idealized physical model and bilinear idealized hysteresis loop of single-concave FP bearing developed in OpenSees

The MYPED was modeled using the Bouc–Wen model [16-18] in OpenSees. Figure 9 shows the force-deformation response of the MYPED.

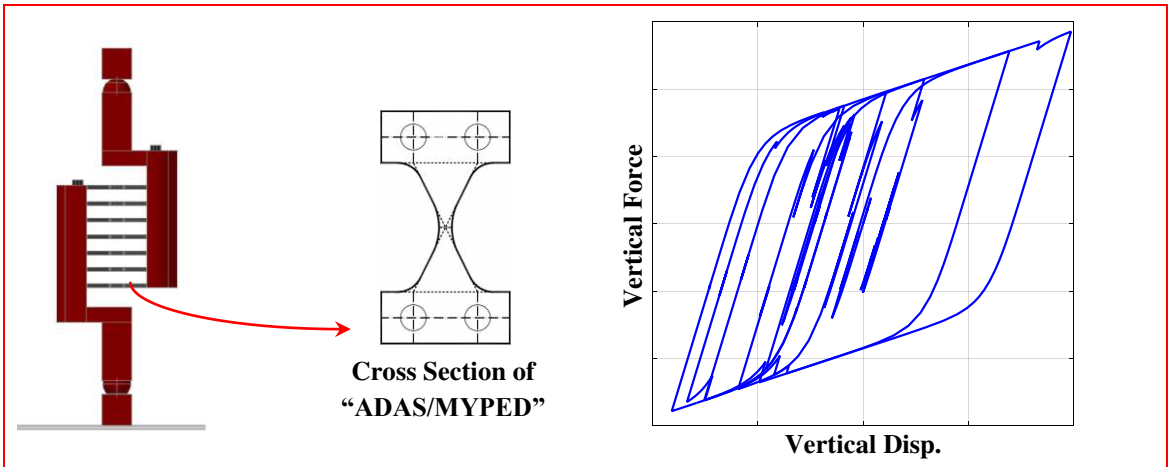

Fig. 9 Telescopic Column, ADAS/MYPED configuration and curvilinear Bouc-Wen hysteresis loop of the TC

Table 2 shows the summary of the structural periods with the three isolation schemes. To make the finite element models more computationally efficient, both the horizontal and vertical masses were lumped in the nodes. 2.5% mass and stiffness proportional Rayleigh damping was assigned in the first 2 modes of vibration.

Table 2: Dominant vibration periods of the reference structures and the isolated systems.

Model	T_1 [sec.]	T_2 [sec.]	T_3 [sec.]
Fixed-Base	0.89	0.24	0.13
Elastomeric Bearing	2.95	0.71	0.32
Friction Pendulum	3.18	0.95	0.41
Telescopic Columns	3.98	1.18	0.57

5. Ground Motion Selection:

Twenty-eight near fault ground motions were selected and amplitude was scaled to match the maximum considered earthquake seismic hazard for the prototype building. Detailed incremental dynamic analysis (IDA) [19] was conducted using these motions. Based on the procedure developed by [20], the selected strong ground motions were classified into 2 subsets as near-field (pulse and no-pulse) records. The selected records have magnitudes in the range of M6.5 to M7.9 and have considerable vertical component and remarkable range of pulse period. Horizontal and vertical response spectra of the selected records are shown in Figure 10.

Table 3. Selected record information and parameters for the near-field pulse subset

ID No.	Earthquake			Recording Station	NEHRP Class	Epicentral distance (km)	Lowest Freq. (Hz)
	M_w	Year	Name				
1	6.5	1979	Imperial Valley-06	El Centro Array #6	D	27.5	0.13
2	6.5	1979	Imperial Valley-06	El Centro Array #7	D	27.6	0.13
3	6.9	1980	Irpinia, Italy-01	Sturno	B	30.4	0.16
4	6.5	1987	Superstition Hills-02	Parachute Test Site	D	16.0	0.15
5	6.9	1989	Loma Prieta	Saratoga - Aloha	C	27.2	0.13
6	6.7	1992	Erzican, Turkey	Erzincan	D	9.0	0.13
7	7.0	1992	Cape Mendocino	Petrolia	C	4.5	0.07
8	7.3	1992	Landers	Lucerne	C	44.0	0.10
9	6.7	1994	Northridge-01	Rinaldi Receiving Sta.	D	10.9	0.11
10	6.7	1994	Northridge-01	Sylmar - Olive View	C	16.8	0.12

11	7.5	1999	Kocaeli, Turkey	Izmit	B	5.3	0.13
12	7.6	1999	Chi-Chi, Taiwan	TCU065	D	26.7	0.08
13	7.6	1999	Chi-Chi, Taiwan	TCU102	C	45.6	0.06
14	7.1	1999	Duzce, Turkey	Duzce	D	1.6	0.10

Table 4. Selected record information and parameters for near-field no-pulse subset

ID No.	Earthquake			Recording Station	NEHRP Class	Epicentral distance (km)	Lowest Freq. (Hz)
	Mw	Year	Name				
15	6.8	6.8	Gazli, USSR	Karakyr	C	12.8	0.06
16	6.5	1979	Imperial Valley-06	Bonds Corner	D	6.2	0.13
17	6.5	1979	Imperial Valley-06	Chihuahua	D	18.9	0.06
18	6.8	1985	Nahanni, Canada	Site 1	C	6.8	0.06
19	6.8	1985	Nahanni, Canada	Site 2	C	6.5	0.13
20	6.9	1989	Loma Prieta	BRAN	C	9.0	0.13
21	6.9	1989	Loma Prieta	Corralitos	C	7.2	0.25
22	7.0	1992	Cape Mendocino	Cape Mendocino	C	10.4	0.07
23	6.7	1994	Northridge-01	LA - Sepulveda VA	C	8.5	0.12
24	6.7	1994	Northridge-01	Northridge - Saticoy	D	3.4	0.13
25	7.5	1999	Kocaeli, Turkey	Yarimca	D	19.3	0.09
26	7.6	1999	Chi-Chi, Taiwan	TCU067	C	28.7	0.04
27	7.6	1999	Chi-Chi, Taiwan	TCU084	C	8.9	0.25
28	7.9	2002	Denali, Alaska	TAPS Pump Sta. #10	C	7.0	0.03

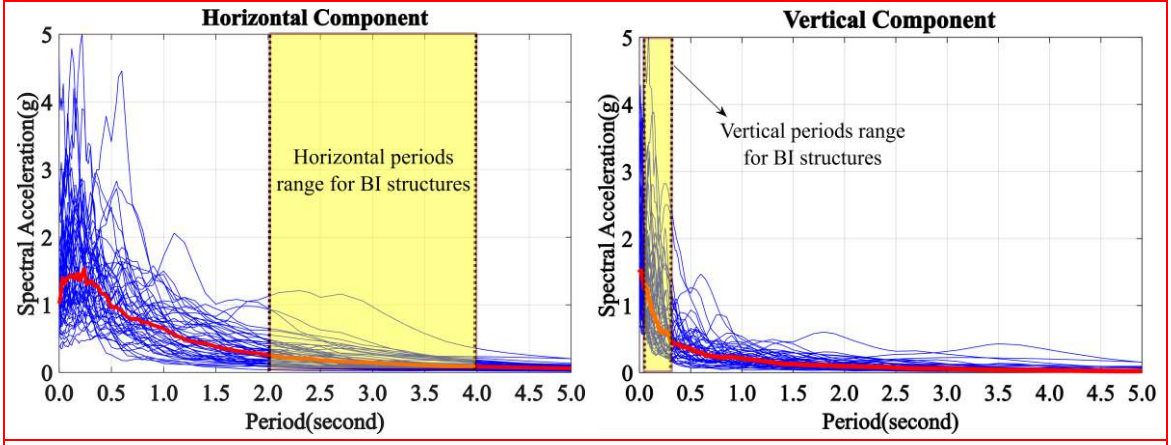

Fig. 10 5% damping, earthquake response spectra for horizontal and vertical components of selected records

6. Selected Damage Index for Performance Evaluation:

In the conventional seismic performance evaluation studies, displacement-based criteria such as inter-storey drift ratio (IDR) may be considered as an appropriate engineering demand parameter (EDP) [21,22]. However, in the current study, the modified Park-Ang damage model [23], which uses a weighting average with respect to combined displacement and absorbed energy of each element, as defined in Eqn. (8) is used.

$$DI_{(P.A)} = \frac{\phi_m - \phi_y}{\phi_u - \phi_y} + \frac{\beta_e}{M_y.\phi_u}\int dE \qquad (8)$$

where ϕ_m is taken from the maximum curvature at each element edge; β_e is the coefficient for structural type which is assumed to be 0.15 in this study. The integral part of the second term is the energy under the M- ϕ hysteretic diagram; ϕ_u is the ultimate curvature of the component; ϕ_y and M_y are the yield curvature and yield moment, respectively.

After the occurred damage at each element is calculated, the global damage of story and building is calculated using Eqns. (9) and (10):

$$DI_{Storey} = \sum \left(\frac{E_i}{\Sigma E_i} \right)_{element} \times (DI_i)_{element} \quad (9)$$

$$DI_{Building} = \sum \left(\frac{E_i}{\Sigma E_i} \right)_{Storey} \times (DI_i)_{Storey} \quad (10)$$

Performance level classifications for the RC-MRFs based on the utilized damage index are presented in Table 5. Regarding to the scope of the current study, only collapse damage mode is used to estimate the seismic fragilities.

Table 5: RC building damage state based on modified Park-Ang DI

Damage State	Qualitative Definition	Damage Range	Best Estimate
Non-Structural	No damage or localised minor cracking	0.01-0.10	0.05
Slight	light cracking throughout	0.10-0.20	0.15
Moderate	severe cracking, localised spalling	0.20-0.50	0.35
Extensive	crushing of concrete, reinforcement exposed	0.50-0.85	0.67
Collapse	-	0.85-1.15	1.00

7. Results and Discussions:

7.1 Optimal Design of the Proposed System:

Based on the formulation presented in section 2, the optimal diameter and height of the RMCC are selected as 120cm and 100cm, respectively. The ADAS/MYPED elements in TCs should be designed efficiently as their elastic and plastic stiffness and yield strain are the main controlling parameters for the energy dissipating mechanisms of these elements. On this basis, the optimal geometric values and the controlling parameters for each X-plate ADAS element used in TCs are calculated for the considered 4-storey RC-MRF using a series of NL analyses. The final appropriate values for each ADAS/MYPED element in TCs are depicted in Figure 11.

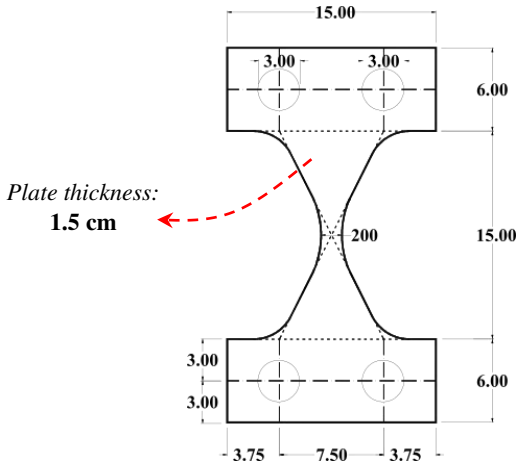

Fig. 11 Cross section of X-plate ADAS element in TCs with optimal dimensions in cm

7.2 Structural response:

The effectiveness of the base isolated systems was evaluated based on four key performance indicators. The peak absolute acceleration (PAA), inter-storey drift ratio (IDR), base shear (V) and axial load (N) were investigated and compared. The seismic performance of the superstructure under combined horizontal and vertical excitations was analyzed using the ground motions presented in Tables 3 and 4. In order to analyze the effects of vertical ground motion, the nonlinear response history analysis (NL-RHA) with (H+V) and without vertical component (H) was carried out. The vertical component was amplified using the same scaling factor, where the V/H ratio is limited to 2.0. Figure 12 shows the absolute roof acceleration of the prototype building under the Loma Prieta earthquake record. The result shows that the maximum roof acceleration was 1.32 g and 1.67 g for H and H+V, respectively. By comparison of the peak absolute acceleration, the base isolated structures have substantially lower response. The peak absolute acceleration for the TCs was 0.22 g and 0.37 g for H and H+V, respectively. This is relatively lower compared to conventional BI systems. Table 6 shows the mean peak absolute accelerations when compared with a fixed-base structure. The results show that the base-isolated response ranged between 14% to 27% and 21% to 33% of the fixed-base structure for the H and H+V excitations, respectively. Based on the results presented, it is concluded that the peak response between the stories was relatively consistent for the base-isolated structures, whereas a substantial increase exists between stories for the fixed-base structure.

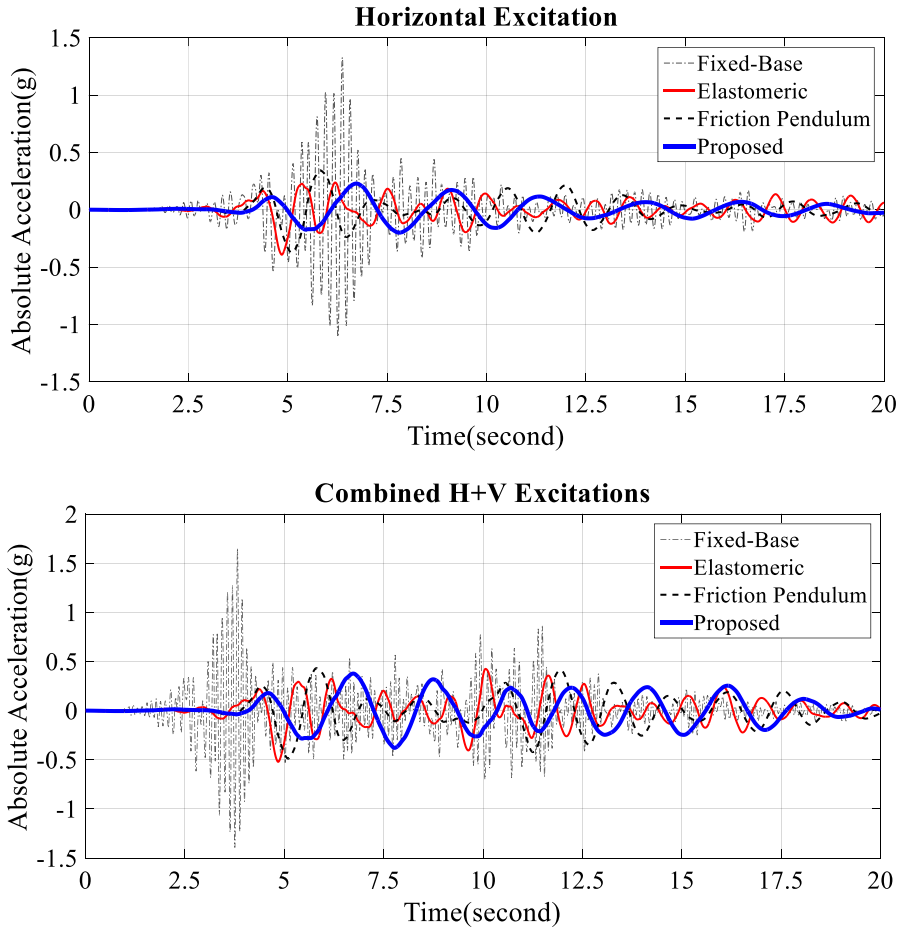

Fig. 12 Top storey acceleration response to Loma Prieta earthquake for horizontal and H+V cases considering various base-isolating systems

Table 6: Mean peak absolute acceleration difference under H and H+V excitations compared to fixed-base structure

Records Type	**Loading**	**EB**	**FP**	**TC**
Pulse Subset	H	25%	27%	15%
	H+V	33%	29%	24%
No-Pulse Subset	H	18%	22%	14%
	H+V	31%	28%	21%

Figs. 13 to 15 illustrate the base shear history of the FPS, EB and TC isolation systems under the Loma Prieta earthquake, respectively. The results show that the vertical component of earthquake places a significant role in the base shear of the structure.

Table 7 shows the mean peak base shear range for the base-isolated systems under Pulse and No-Pulse subsets. The results show that for the BI structures considering only the horizontal seismic loads, the superstructure design is underestimated. The most vulnerable case is the superstructure designed on the friction pendulum bearing and the least one is the building mounted on the proposed system.

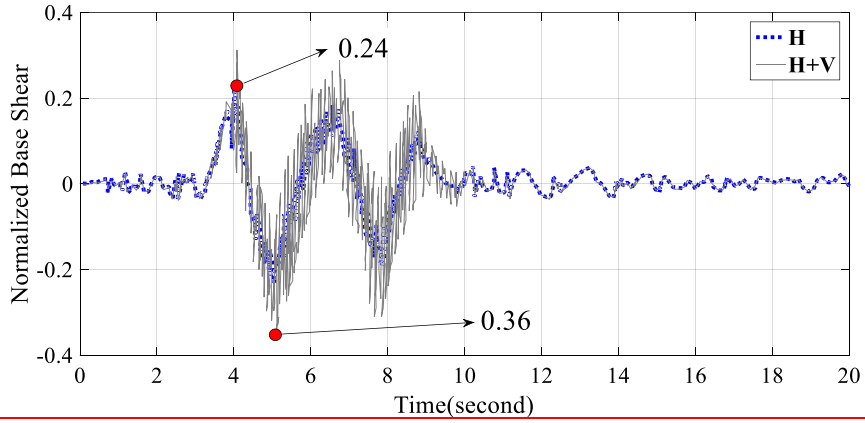

Fig. 13 Normalized base shear time history for BI with friction pendulum under Loma Prieta earthquake

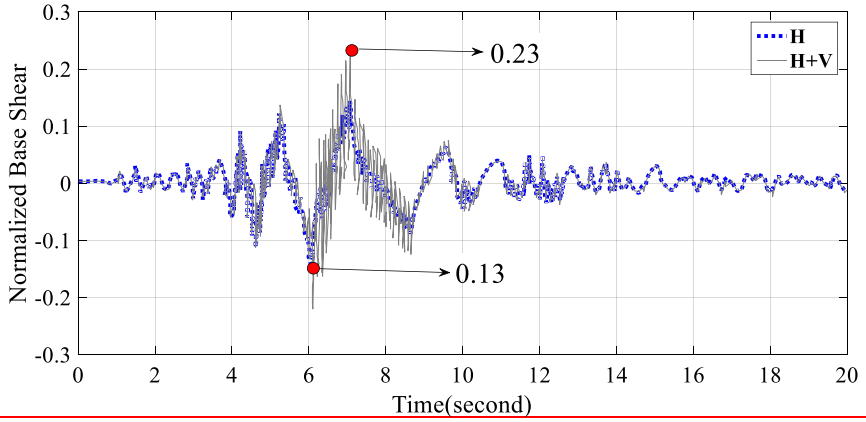

Fig. 14 Normalized base shear time history for BI with elastomeric bearing under Loma Prieta earthquake

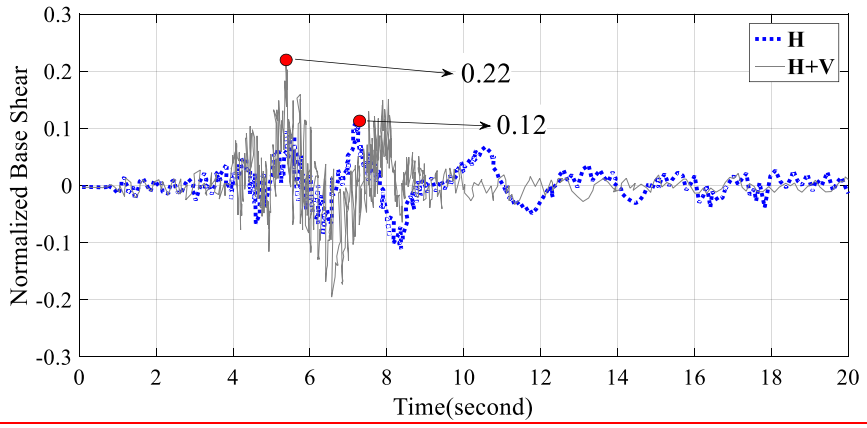

Fig. 15 Normalized base shear time history for BI with telescopic columns under Loma Prieta earthquake

Table 7. Mean peak base shear range for the base isolated systems under pulse and no-pulse subsets

Records Type	**Loading**	**EB**	**FP**	**TC**
Pulse Subset	H	(0.18-0.29) g	(0.21-0.32) g	(0.16-0.21) g
	H+V	(0.23-0.35) g	(0.26-0.43) g	(0.19-0.28) g
No-Pulse Subset	H	(0.11-0.25) g	(0.18-0.30) g	(0.09-0.15) g
	H+V	(0.20-0.31) g	(0.22-0.38) g	(0.14-0.24) g

Figs. 16-18 show the comparison of IDRs under both horizontal and combined seismic excitations. The result shows that the maximum inter-storey displacement (ISD) and IDR usually occur over the first storey of the superstructure. This is attributed to a larger cumulated shear at this level. Based on the NL-RHA, the average maximum ISDs for the fixed-base structure were (37-61) mm and (46-88) mm for horizontal and combined H+V, respectively. Table 8 shows the summary of the mean peak ISD and IDR for the superstructure under pulse and non-pulse subsets. Regardless of the low ISD and IDR values, the base-isolated structure displayed a desirable reduction with values ranging between 7.6% and 16.5% of the fixed-base values. Similar to the peak absolute acceleration response, it can be observed that the peak ISD and IDR for the proposed system were lower than the elastomeric bearing and friction pendulum in all instances.

Table 8: Peak ISD and IDR for the superstructure equipped with BI systems under pulse and non-pulse subsets

Records Type	**Loading**	**FB**		**EB**		**FP**		**TC**	
		ISD(mm)	IDR(%)	ISD(mm)	IDR(%)	ISD(mm)	IDR(%)	ISD(mm)	IDR(%)
Pulse Subset	H	60.80	1.52	8.80	0.22	6.00	0.15	4.80	0.12
	H+V	88.40	2.21	12.40	0.31	11.20	0.28	6.80	0.17
No-Pulse Subset	H	36.80	0.92	5.20	0.13	4.80	0.12	2.80	0.07
	H+V	46.00	1.15	6.80	0.17	7.60	0.19	4.40	0.11

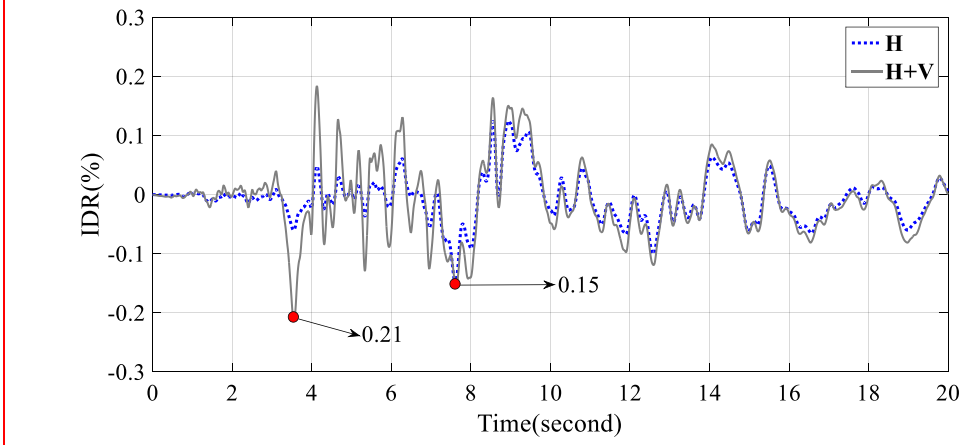

Fig. 16 IDR time history for BI with elastomeric bearing under Loma Prieta earthquake.

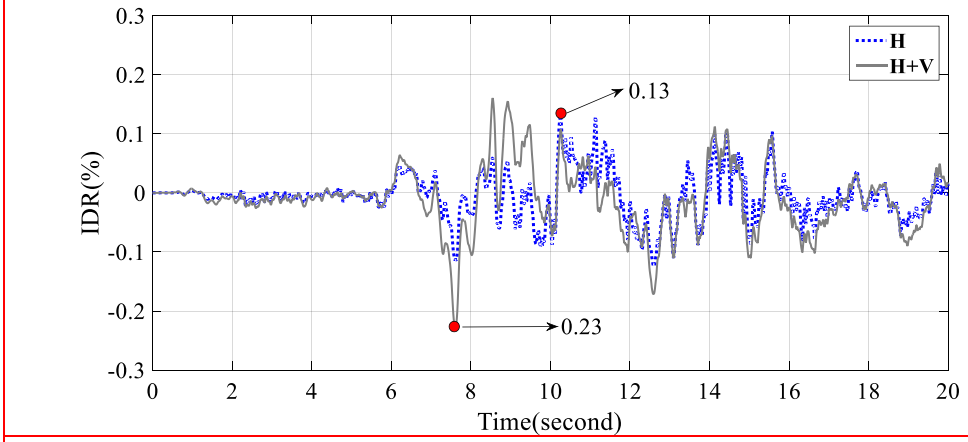

Fig. 17 IDR time history for BI with friction pendulum under Loma Prieta earthquake.

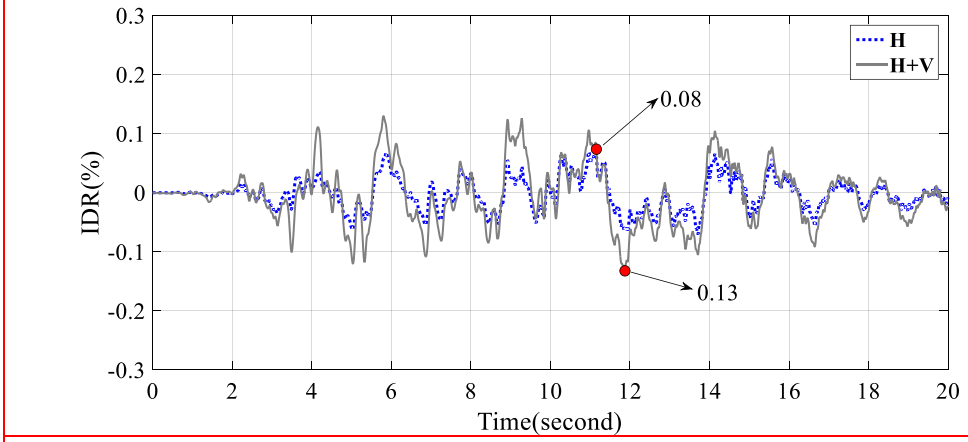

Fig. 18 IDR time history for BI with telescopic columns under Loma Prieta earthquake.

Another important phenomenon, which happens in the presence of vertical excitation, is the significant fluctuation of axial force. This increases the possibility of the shear failure in the columns, especially in the first storey of the superstructure. To this end, the focus has been on the attained axial loads by the columns, to check if failure occurs. Figs. 19 to 21 show the variation of the averaged maximum values of the axial loads of the columns on each floor under all selected earthquake records with different V/H ratio utilizing various BI systems.

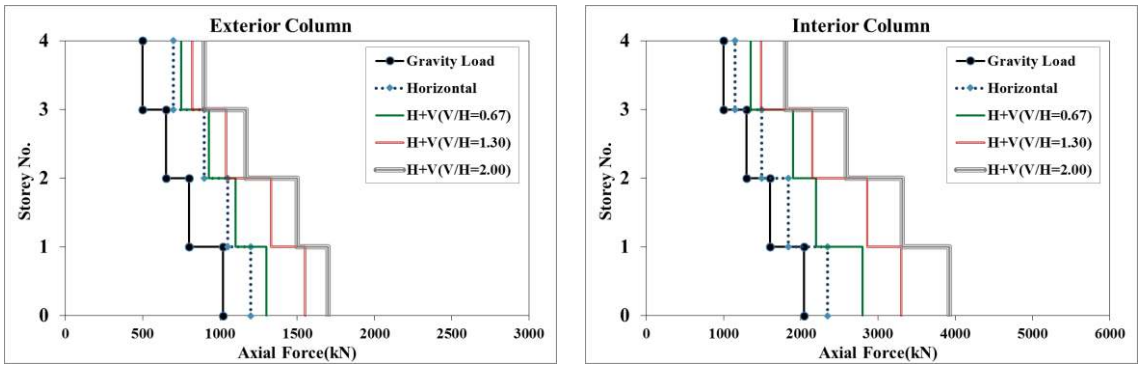

Fig. 19 Average peak axial force in the superstructure columns equipped with elastomeric bearing BI system

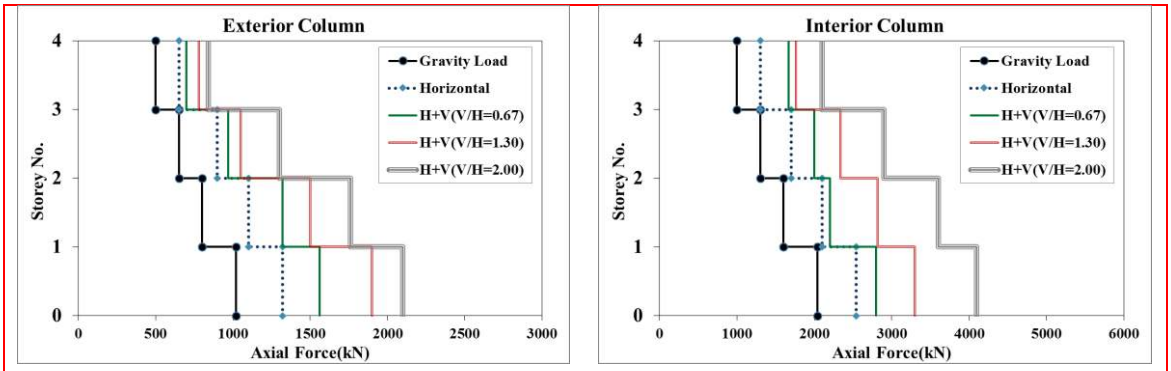

Fig. 20 Average peak axial force in the superstructure columns equipped with friction pendulum BI system

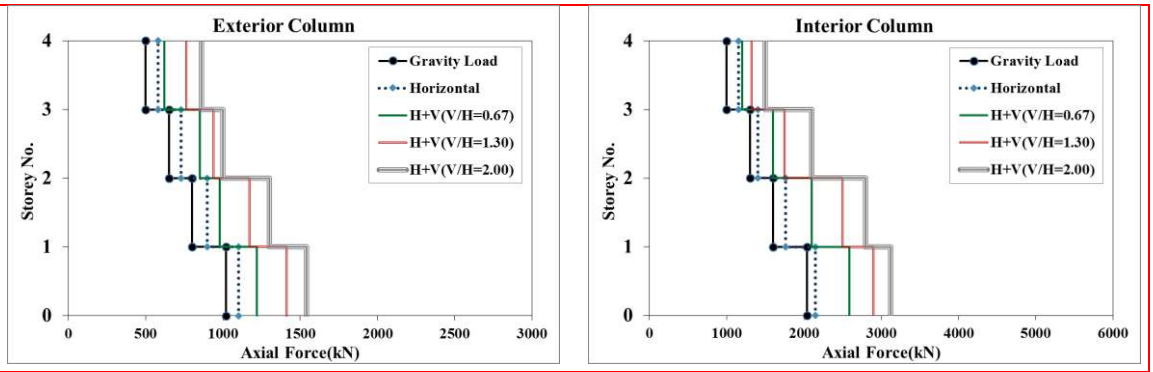

Fig. 21 Average peak axial force in the superstructure columns equipped with proposed BI system

From the results presented, it comes out that both exterior and interior columns undergo critical conditions while subjecting to combined H+V excitations, especially at the lower stories. In particular, for V/H ratios large enough (even for the value V/H=0.67, corresponding to the current design philosophy in the seismic design codes), the axial demand exceeds the axial capacity of the columns at the lower stories. This increment is the most for the friction pendulum case and the least for the proposed system, which shows the high seismic performance of the new system in the presence of vertical excitations.

A marked increase of the axial-load variation occurs when the vertical component of the selected records (V/H=2.00) is taken into account: in both the interior and exterior columns of the first story, the axial load reaches a value of about twice as large as the corresponding gravity loading value. In this regard, it should be noted that the tributary mass corresponding to an interior column is greater than that for an exterior column; thus, the seismic effects due to the vibrations along the vertical direction in the interior column are greater than those in an exterior column.

7.3 Seismic Fragility Estimation:

The collapse margin ratio for the prototype model was analyzed using the IDA analysis as outlined in FEMA P-695 procedure [24]. The limit state for each damage mode is defined previously based on modified Park-Ang damage index. The intensity measure (IM) in the analyses and fragility estimation is assumed to be a scale factor relative to the MCE spectrum intensity at the first mode period of fixed base and BI structures ($Sa_{\text{(Fixed Base)}}$ = 2.21g, $Sa_{\text{(Elastomeric)}}$ = 0.43g, $Sa_{\text{(Friction Pendulum)}}$ = 0.38g, $Sa_{\text{(Telescopic Columns)}}$ = 0.31g), such that an intensity scale factor (ISF) of 1.0 represents the MCE intensity at the fundamental period of the model. To consider the influence of vertical component of ground motions on the collapse fragilities, a different V/H ratio is considered. Figure 22 shows the fragility curves for the proposed models. The result shows that using base-isolating (EB, Fp or TC) techniques can significantly reduce the probability of collapse. By comparing the fragility curves for various BI systems, a higher collapse potential is evident in the case of elastomeric bearing and friction pendulum compared to TCs. As the V/H ratio increases, the probability of collapse increases. By comparing the EB and FP system, the EB is more vulnerable than FP by about 8% and 17% for the H and H+V cases, respectively.

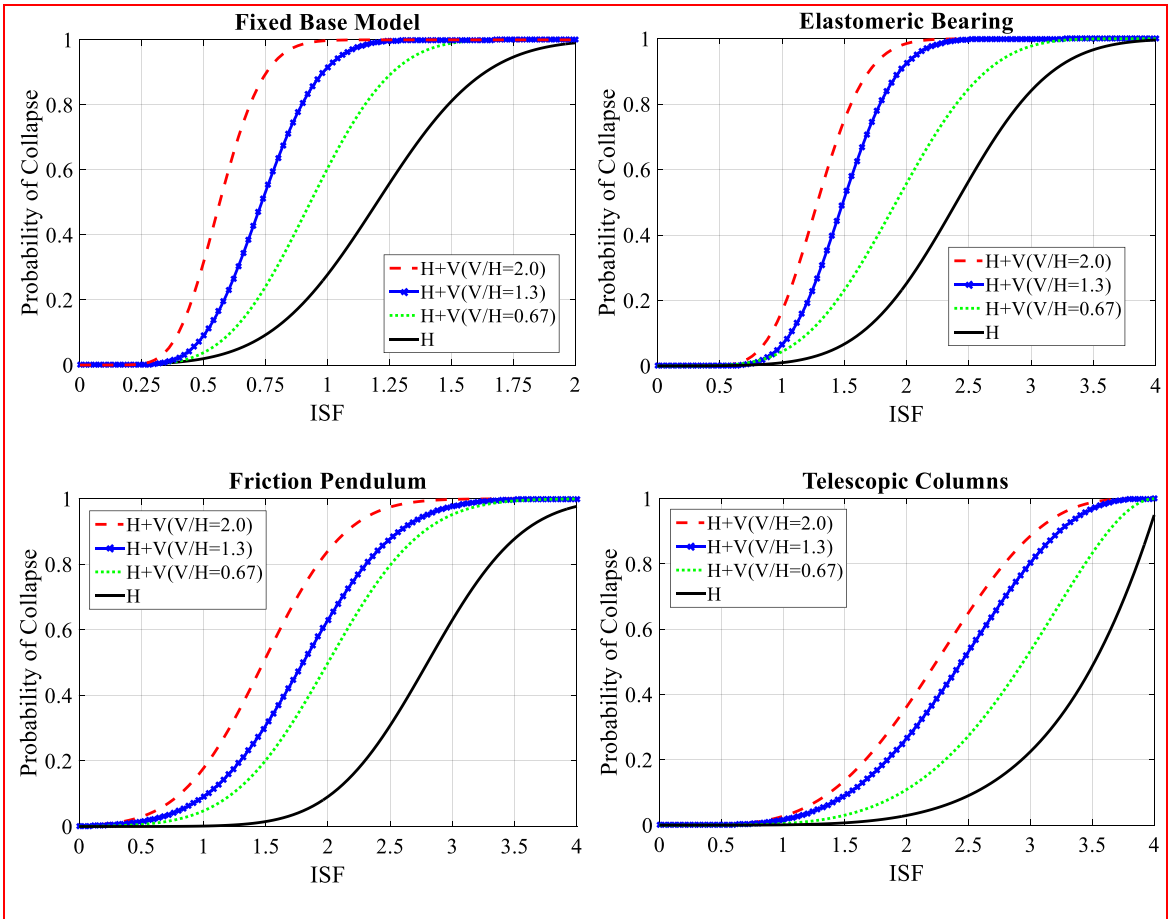

Fig. 22 Fragility curves for fixed-base and BI RC-MRF under H and H+V excitations

7.4 Performance Evaluation:

Similarly, using the FEMA P-695 procedure [24], the adjusted collapse margin ratio (ACMR) was analyzed. The ACMR was compared with the acceptable ACMR shown in Table 9 and Figure 23. The result shows that the ACMR reduction is very pronounced for all the models under an increasing V/H ratio. In the case of fixed-base RC-MRF, the system has unacceptable response when the V/H exceeds 1.3. On the other hand, the conventional BI systems, both EB and FP passed the acceptable ACMR, while for the high amplitude of vertical excitation which is underestimated in the current seismic codes, the systems are in a marginal condition. Analyses show that reductions in ACMR are more substantial for the EB when compared with the FP and the TC system. The results indicate that, BI systems have comparable levels of safety to code-conforming, conventional fixed-base structures. Even though, it should be noted that the code criteria for base-isolated systems are adequate, and may be conservative in the case of horizontal excitations, but need some modifications to consider the effect of high vertical excitations in the near-fault regions. It is also worth mentioning that the TC system is relatively safer compared to conventional BI systems and can be used as an appropriate and reliable vibration control system for the structures located in high seismic zones with significant vertical excitation.

Table 9: Calculation of ACMRs for fixed-base and BI systems considering vertical component with multiple V/H ratios

Model	Loading	Computed Collapse Margin Ratio			Acceptable ACMR	Performance
		CMR	SSF	ACMR		
Fixed-Base	**H**	1.21	1.44	1.74	1.34	Safe
	H+V(V/H:0.67)	0.94	1.44	1.35	1.34	Marginal
	H+V(V/H:1.3)	0.74	1.44	1.07	1.34	Un-Safe
	H+V(V/H:2.0)	0.57	1.44	0.82	1.34	Un-Safe
Elastomeric Bearing	**H**	2.4	1.21	2.90	1.52	Safe
	H+V(V/H:0.67)	1.92	1.21	2.32	1.52	Safe
	H+V(V/H:1.3)	1.5	1.21	1.82	1.52	Safe
	H+V(V/H:2.0)	1.27	1.21	1.54	1.52	Marginal
Friction Pendulum	**H**	2.79	1.21	3.38	1.52	Safe
	H+V(V/H:0.67)	1.98	1.21	2.40	1.52	Safe
	H+V(V/H:1.3)	1.8	1.21	2.18	1.52	Safe
	H+V(V/H:2.0)	1.48	1.21	1.79	1.52	Safe
Telescopic Columns	**H**	3.52	1.21	4.26	1.52	Safe
	H+V(V/H:0.67)	2.95	1.21	3.57	1.52	Safe
	H+V(V/H:1.3)	2.44	1.21	2.95	1.52	Safe
	H+V(V/H:2.0)	2.24	1.21	2.71	1.52	Safe

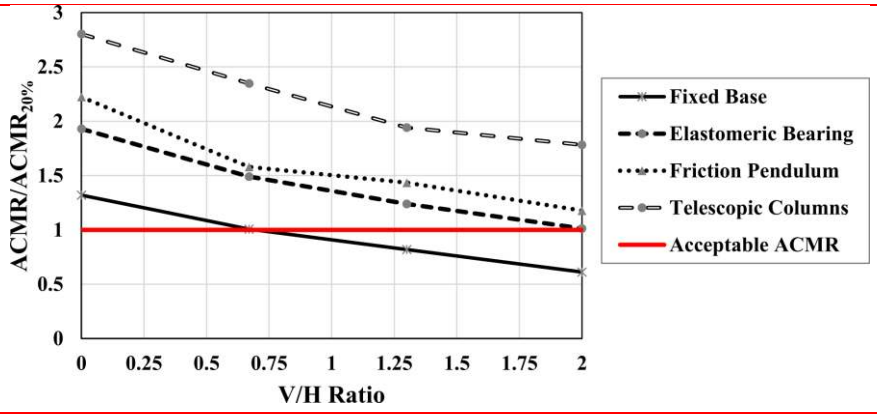

Fig. 23 Ratio of calculated ACMR to acceptable ACMR for 20% probability of collapse

8. Conclusions:

With increasing concern of the earthquake excitation with vertical component, an advanced TC base-isolated system was proposed in this paper. A detailed seismic performance and nonlinear response of a RC-MRF equipped with elastomeric bearing (EB), friction pendulum (FP) and a proposed telescopic column (TC) isolation systems have been investigated under a large dataset of near-fault ground motions. The effects of the vertical component of motion were emphasized considering cases in which a horizontal component of motion is assumed acting alone or simultaneously with the vertical one.

The collapse fragility curves which are the main requirement of earthquake loss assessment were produced and collapse margin ratios of the models with various influencing parameters were evaluated. Unlike the conventional BI systems, the TC system proves effective for controlling the damage of RC frame members, producing an elongation of the effective fundamental vibration period and controlling both horizontal (H) and (H+V) excitations. From the above discussions, the following conclusions can be drawn:

1. In the current study, unlike the common approach which models the superstructure as a simplified MDOF elastic system, a more complicated and concentrated plasticity approach was utilized to consider the effect of cyclic deterioration on the superstructure elements. The results proved the high accuracy of the implemented approach in terms of combined H+V excitations.
2. The first two mode periods of the system equipped with telescopic columns are 3.98s and 1.18s, respectively. This is longer than the periods of elastomeric bearing and friction pendulum systems. This is mainly because of the rocking motion of the TC system, which leads to longer periods and, therefore, lower acceleration values in the buildings. This not only results in reduction of the seismic forces imposed to the building system, but also provides higher safety level of non-structural elements in the superstructure.
3. The NL-RHA depicted that in the case of combined H+V excitation, the axial force in columns, tip floor acceleration, ISD, IDR and the base shear values are significantly amplified compared to the case of horizontal only excitation.
4. On the deterministic part, the overall responses of the BI RC-MRF are seen to be much amplified when the model is excited by the Pulse subset in FEMA P-695 compared to the No-Pulse dataset. It can be inferred that ground motions including the forward directivity effect can cause severe damage and hazards to the BI systems. This fact necessitates the careful classification and selection of ground motions for seismic risk assessment of BI structures which can expose the stronger effects of earthquakes with high velocity pulses.
5. Another important finding is that the multi-component seismic excitations including vertical component may increase the compressive and tensile axial force/stress in the columns. This increment may cause crushing/buckling damage or lead to annular cracks in the members

because of the significant reduction in shear capacity, which alter the collapse mode of the element from flexural to shear failure. Herein, the columns are more susceptible to this type of failure for high amplitude of vertical component of ground motion.

6. On the probabilistic part, this study illustrates the application of the FEMA P-695 methodology to isolated structures, which have fundamentally different dynamic response characteristics, performance properties and collapse failure modes than those of conventional, fixed-base structures. It demonstrates that, when evaluated in accordance with the methodology, base-isolated systems provide levels of safety against collapse that are comparable to conventional, fixed-base structures. It should also be noted that the proposed system produced larger ACMR values compared to conventional BI devices, which leads to a more reliable seismic behavior of building structures.

In conclusion, the vertical component of earthquake ground motions should be accounted for in the seismic design of structures, even when the structure is seismically isolated. The proposed TC system provides efficient easiness of manufacturing and installation, which can be used efficiently to mitigate the seismic vulnerability of mid-rise multi-story buildings.

Nomenclature:

The following symbols are used in this paper:

References:

[1] Skinner RI, Robinson WH, McVerry GH. An introduction to seismic isolation. John Wiley & Sons; 1993.
[2] Yang TY, Konstantinidis D, Kelly JM. The influence of isolator hysteresis on equipment performance in seismic isolated buildings. Earthquake Spectra. 2010 Feb;26(1):275-93.
[3] Chen X, Yang TY, Shi W. Influence of isolation hysteresis on the seismic performance of isolated buildings. Structural Control and Health Monitoring. 2015 Apr 1;22(4):631-47.
[4] Stenswick LE, inventor. Seismic isolation system. United States patent US 9,222,276. 2015 Dec 29.
[5] Kageyama M, Iba T, Umeki K, Somaki T, Hino Y, Moro S, Ikutama S. Study on three-dimensional seismic isolation system for next generation nuclear power plant: independent cable reinforced rolling-seal air spring. InProceedings of the 13th World Conference on Earthquake Engineering 2004 Jan 1.
[6] Yoo, B., Lee, J. H., Koo, G. H. and Kim, Y. H. A study of vertical seismic responses for base isolated PWR using high damping rubber bearing, 14th International conference on Structural Mechanics in Reactor Technology, Lyon, France 1997.
[7] Sato E, Furukawa S, Kakehi A, Nakashima M. Full-scale shaking table test for examination of safety and functionality of base-isolated medical facilities. Earthquake Engineering & Structural Dynamics. 2011 Oct 25;40(13):1435-53.
[8] Ryan, K.L., Dao, N., Siavash, S., Manos, M., Eiji, S., Tomohiro, S. and Arash, Z. Seismic Interaction of Structural System and Non-structural Components in the NEES TIPS/NEES Nonstructural/NIED Collaborative Tests at E-Defense, Proc. 2012 ASCE Structures Congress, Chicago, IL 2012.
[9] Hosseini M, Farsangi EN. Telescopic columns as a new base isolation system for vibration control of high-rise buildings. Earthquakes and Structures. 2012;3(6):853-67.
[10] Tsai KC, Chen HW, Hong CP, Su YF. Design of steel triangular plate energy absorbers for seismic-resistant construction. Earthquake spectra. 1993 Aug;9(3):505-28.

[11] Shih MH, Sung WP. A model for hysteretic behavior of rhombic low yield strength steel added damping and stiffness. Computers & structures. 2005 May 31;83(12):895-908.
[12] Pacific Earthquake Engineering Research Center (PEER). Open System for Earthquake Engineering Simulation (OpenSees) 2014.
[13] ACI Committee 318. Building Code Requirements for Reinforced Concrete (ACI 318-89) and Commentary-ACI 318-89. American Concrete Institute.
[14] Haselton CB, Goulet CA, Mitrani-Reiser J, Beck JL, Deierlein GG, Porter KA, Stewart JP, Taciroglu E. An assessment to benchmark the seismic performance of a code-conforming reinforced-concrete moment-frame building. Pacific Earthquake Engineering Research Center. 2008(2007/1).
[15] Elwood KJ. Modelling failures in existing reinforced concrete columns. Canadian Journal of Civil Engineering. 2004 Oct 1;31(5):846-59.
[16] Bouc R. A mathematical model for hysteresis. Acta Acustica united with Acustica. 1971 Jan 1;24(1):16-25.
[17] Wen YK. Method for random vibration of hysteretic systems. Journal of the engineering mechanics division. 1976 Apr;102(2):249-63.
[18] Park YJ, Wen YK, Ang A. Random vibration of hysteretic systems under bi-directional ground motions. Earthquake engineering & structural dynamics. 1986 Jul 1;14(4):543-57.
[19] Vamvatsikos D, Cornell CA. Incremental dynamic analysis. Earthquake Engineering & Structural Dynamics. 2002 Mar 1;31(3):491-514.
[20] Baker JW. Quantitative classification of near-fault ground motions using wavelet analysis. Bulletin of the Seismological Society of America. 2007 Oct 1;97(5):1486-501.
[21] Taghavi S, Miranda E. Response assessment of nonstructural building elements. Pacific Earthquake Engineering Research Center; 2003.
[22] Cutfield M, Ryan K, Ma Q. Comparative life cycle analysis of conventional and base-isolated buildings. Earthquake Spectra. 2016 Feb;32(1):323-43.
[23] Williams MS, Sexsmith RG. Seismic damage indices for concrete structures: a state-of-the-art review. Earthquake spectra. 1995 May;11(2):319-49.
[24] FEMA P. 695. Quantification of Building Seismic Performance Factors. Federal Emergency Management Agency. 2009 Jun.